Chemical Science

EDGE ARTICLE

View Article Online
View Journal | View Issue

Open Access Article. Published on 18 Mai 2015. Downloaded on 02.02.2026 10:12:41.
This article is licensed under a Creative Commons Attribution-NonCommercial 3.0 Unported Licence.

CrossMark click for updates

Cite this: *Chem. Sci.*, 2015, **6**, 4350

Synthesis of open-mouthed, yolk–shell Au@AgPd nanoparticles with access to interior surfaces for enhanced electrocatalysis†

Qiurong Shi,[a] Peina Zhang,[a] Yijing Li,[a] Haibing Xia,*[a] Dayang Wang[b] and Xutang Tao[a]

Received 26th March 2015
Accepted 16th May 2015

DOI: 10.1039/c5sc01088h

www.rsc.org/chemicalscience

We have successfully produced open-mouthed, yolk–shell (OM-YS) Au@AgPd nanoparticles (NPs) *via* galvanic replacement reaction at room temperature; each NP has a large opening on its AgPd shells. Owing to the openings on the AgPd shells, the inner surfaces of the AgPd shells of as-prepared OM-YS Au@AgPd NPs become accessible to the surrounding media. These new structural characters make the present OM-YS Au@AgPd NPs excellent catalysts for electrochemical oxidation of ethanol in alkaline media. Their electrochemical active surface area is 87.8 $m^2\ g^{-1}$ and the mass activity is 1.25 A mg_{Pd}^{-1}. Moreover, the openings on the AgPd shells also make the surfaces of the Au cores in OM-YS Au@AgPd NPs accessible to the reaction media, which significantly facilitates the removal of CO and other carbonaceous intermediate species, thus leading to substantially enhanced durability and stability. This superior electrocatalytic performance cannot be implemented by using conventional YS Au@AgPd NPs or commercially available Pd/C catalysts.

Introduction

Pd-based catalysts exhibit an excellent electrocatalytic performance in ethanol oxidation in alkaline media.[1,2] It is known that the introduction of Au into the Pd-based catalysts can effectively eliminate intermediates, *e.g.* CO, by oxidation and thus improve the Pd resistance to poisoning.[3,4] Thus, Pd/Au composite nanoparticles (NPs) with bimetallic alloy and core–shell (CS) structures have been successfully developed to catalyze various electrochemical reactions.[5–10] However, they lead almost no real improvement in Pd catalysis performance as compared with Pd nanoparticles because these structures still rely on the exterior surfaces of Pd shells to perform the electrocatalysis, very similar to conventional Pd nanoparticles. Moreover, it is still expensive to utilize especially when the use of Au does not add any value in catalysis. Yolk–shell (YS) metallic NPs are a special type of core–shell structured NPs, in which there are distinct gaps interspaced between the cores and shells, which leads to new properties, usually not expected for conventional core–shell NPs.[11–13] However, since both CS or YS Au@AgPd NPs have intact AgPd shells enclosing Au cores, the functions of the Au cores are hardly integrated with that of the AgPd shells in technical applications, *e.g.* catalysis. Therefore, integration of the catalytic behaviour of the both exterior and interior surfaces of AgPd shells and that of Au cores or yolks become an increasingly pressing topic in this research field. Recently, the synthesis of hollow nanoframes has been reported, which allow their exterior and interior surfaces to be easily accessed for catalysis.[14] Up to date, nanopores (1–2 nm) on the AgPd shells of YS Au@AgPd NPs are useful for drug delivery and lithium-ion batteries, however, they did not lead to large improvement in catalytic performance because the pore dimension is close to the mean free path of organic reactant molecules, thus leading to large diffusion resistance.[15] The El-sayed group also proposed that nanocatalysts should show high chemical activity, high surface area, high degree of roughness, less capping materials, and hollow structure having suitable cavity size with the appropriate number and size of the holes on its walls.[16] Currently, YS metallic NPs can be easily fabricated *via* galvanic replacement reactions.[17] Up to date, galvanic replacement reactions are usually conducted at high temperature in order to increase the solubility of insoluble precipitates, *e.g.* AgCl when silver shells are used as sacrificial templates and thus ensure well-defined YS morphology. Only recently, surfactants such as cetyltrimethylammonium bromide have been utilized as complexing agents to aid insoluble precipitates such as AgCl

[a]*State Key Laboratory of Crystal Materials, Shandong University, Jinan, 250100, P. R. China. E-mail: hbxia@sdu.edu.cn*

[b]*Ian Wark Research Institute, University of South Australia, Adelaide, SA 5095, Australia*

† Electronic supplementary information (ESI) available: Detailed experimental procedure, supplementary TEM images and UV-vis spectra of as-prepared samples, possible formation mechanism of core–shell Au@AgPd NPs, half-encased, core–shell Au@AgPd NPs, conventional yolk–shell Au@AgPd NPs and open-mouthed, yolk–shell Au@AgPd NPs, HAADF-STEM image, HAADF-STEM-EDS images and cross-sectional compositional line profiles of the conventional YS Au@AgPd NPs, UV-vis spectra of conventional and open-mouthed YS Au@AgPd NPs obtained in different solvents of varying refractive indexes, electrocatalytic data of as-prepared samples. See DOI: 10.1039/c5sc01088h

This journal is © The Royal Society of Chemistry 2015

Open Access Article. Published on 18 Mai 2015. Downloaded on 02.02.2026 10:12:41.
This article is licensed under a Creative Commons Attribution-NonCommercial 3.0 Unported Licence.

dissolving in the reaction media, which enabled galvanic exchange reactions to take place at room temperature.[18] Moreover, the use of surfactants for the production of YS Au@AgPd NPs can yield porous AgPd shells.[17,19] However, the removal of the surfactants, AgCl precipitates, and surfactant/AgCl complexes is necessitated prior to use in order to liberate more Pd surfaces for catalysts.[20–23]

Herein we report, to our best knowledge, the first success in fabrication of YS Au@AgPd NPs with single opening (about 20 nm) on the AgPd shell at room temperature. These openings on the AgPd shells allow utilization not only of both the exterior and interior surfaces of the AgPd shells for catalysis, but also of the promotional effect of the Au cores inside to remove CO and thus improve the durability of catalytic performance of the AgPd shells. This new structure is referred to as open-mouthed YS type (OM-YS). As-prepared OM-YS Au@AgPd NPs exhibit superior catalytic activity in ethanol oxidation in alkaline media (1.25 A mg_{Pd}^{-1}) relative to conventional YS Au@AgPd NPs (1.03 A mg_{Pd}^{-1}) and commercial Pd/C catalyst (0.20 A mg_{Pd}^{-1}). The durability is significantly enhanced; 76% of the catalytic activity is retained after a 300 cycle test.

Results and discussion

In this work, CS Au@Ag NPs with controlled Ag thickness were first prepared by hydroquinone (HQ) reduction of $AgNO_3$ on pre-formed citrate-stabilized, 30 nm Au NPs in water at room temperature (Fig. S1 and S2 and Table S1, ESI†). CS or YS Au@AgPd NPs were obtained *via* galvanic exchange reactions at a higher temperature, *e.g.* 60 °C, which was in agreement with literature.[17] It is known that the growth rate of the Pd shell should be significantly reduced at room temperature compared with that at a higher temperature.[18] In our work, we also added an excess of citrate into the reaction media to form Ag–citrate complexes,[24] which increased the diffusion coefficient[18] to facilitate mobility vacancies and jumps of Ag atoms in the Ag shells and dissolution of AgCl precipitates generated during galvanic exchange reaction between Pd^{2+} ions and Ag shell (possible formation mechanism of core–shell Au@AgPd NPs, half-encased, core–shell Au@AgPd NPs, conventional yolk–shell Au@AgPd NPs and open-mouthed, yolk–shell Au@AgPd NPs, ESI†). Here we found that when the thickness of the Ag shells of as-prepared CS Au@Ag NPs was in the range of 3–6 nm, OM-YS Au@AgPd NPs were obtained *via* galvanic replacement reactions at an optimized concentration of citrate in the reaction media at room temperature (Fig. 1, S3–S5 and Table S2, ESI†). Our results suggested that OM-YS Au@AgPd NPs were formed *via* galvanic exchange reaction at the Pd^{2+} to Ag molar ratio in the range of 0.5–1.

Fig. 2a shows the transmission electron microscopy (TEM) image of OM-YS Au@AgPd NPs obtained *via* galvanic reactions of Au@Ag NPs. The gaps between the Au cores and the AgPd shells are clearly visible and most AgPd shells are open-mouthed, in comparison with conventional YS Au@AgPd NPs (Fig. S5c, ESI†). The lattice spacings, marked in the high-resolution TEM (HRTEM) image of the selected area of individual OM-YS Au@AgPd NP (the inset in Fig. 2a), are about 0.228 and 0.235 nm, which are indexed to the (111) planes of the alloyed AgPd shells and Au cores, respectively (Fig. 2b) as the lattice spacing (0.228 nm) is between the interplanar separation of (111) plane of fcc Pd (0.224 nm) and (111) plane of fcc Ag (0.236 nm). The composition of as-prepared OM-YS Au@AgPd NPs (Fig. S6†) was also further characterized by using X-ray diffraction (XRD).

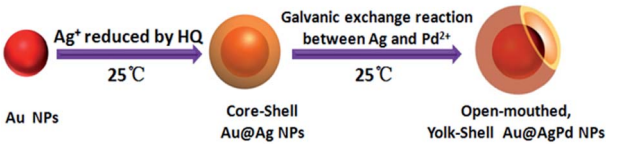

Fig. 1 Schematic representation of the synthetic procedure of open-mouthed, yolk–shell Au@AgPd NPs by galvanic reaction of Au@Ag NPs with Pd^{2+} ions at room temperature.

The diffraction peaks of OM-YS Au@AgPd NPs could be indexed as the (111), (200), (220), (311) and (222) planes of a face-centered cubic (fcc) lattice.[10,25,26] The peak positions were in agreement with those of the pure fcc-structured Au due to the high percentage of Au in the OM-YS Au@AgPd NPs[27] (about 70% on the basis of STEM result below). However, the presence of the peak centred at 81.9°, in between that of pure Ag (81.5°) and that of pure Pd (82.1°) was indicative of the formation of AgPd alloy.[28]

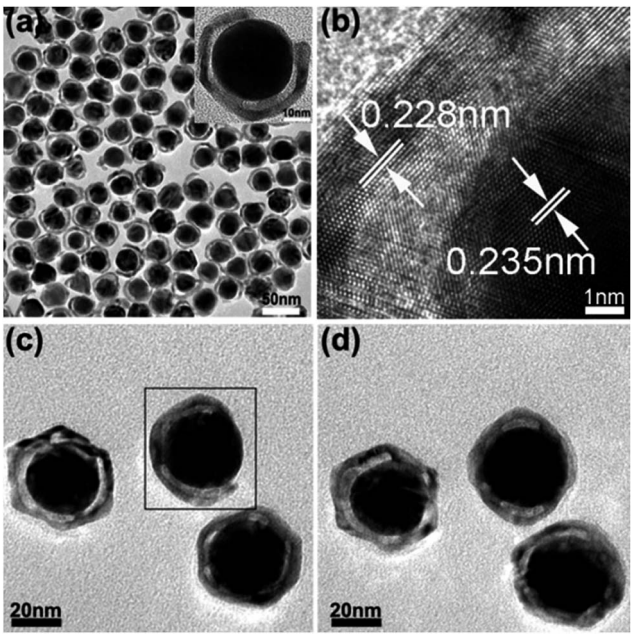

Fig. 2 Low-magnification TEM image (a) of OM-YS Au@AgPd NPs. HRTEM image (b) of the selected area of one individual OM-YS Au@AgPd NP (the inset in (a)). TEM images of an OM-YS Au@AgPd NP taken at different tilting angles from 0 (c) to −20° (d) with respect to the rotation axis. OM-YS Au@AgPd NPs are derived from CS NPs with 30 nm Au NPs and 5.4 nm thick Ag shells *via* galvanic reactions at room temperature. The Pd^{2+} to Ag molar ratio is 0.5 and the citrate concentration is 0.03 wt%.

Open Access Article. Published on 18 Mai 2015. Downloaded on 02.02.2026 10:12:41.
This article is licensed under a Creative Commons Attribution-NonCommercial 3.0 Unported Licence.

It seems that not all YS Au@AgPd NPs are open-mouthed (Fig. 2a and S7†). Thus, a set of TEM images of as-prepared OM-YS Au@AgPd NPs are recorded at different tilting angles, −20 and 0° with respect to the axis of rotation (Fig. 2c and d). It reveals the appearance and disappearance of open-mouths of YS Au@AgPd NPs under TEM observation. Thus, we believe that the disappearance of the open-mouths, shown in Fig. 2a, is due to the different tilting angles of individual OM-YS Au@AgPd NPs on copper grids.

TEM three-dimensional (3D) tomography of a single OM-YS Au@AgPd NP was also implemented by imaging the NP at different specimen orientations. Fig. 3a is the corresponding image of Au@AgPd NPs after TEM 3D reconstruction, in which the inner Au yolk and the outer AgPd shell are shown as red and white color, respectively. One clear open-mouth with a stereoscopic effect can be observed *via* rotating the *x*, *y* or *z* axis under appropriate visual angle (Fig. 3b and Movie S1, ESI†). High-angle annular dark field-scanning TEM (HAADF-STEM) 3D tomography imaging of a single OM-YS Au@AgPd NP was obtained *via* imaging the NP at different specimen orientations in order to reconstruct a 3D tomography with surface view. Fig. 3c reveals that the AgPd surface of the OM-YS NPs is rather rough (Movie S2, ESI†). The HRTEM image of the edge of the curved region of the AgPd shell (Fig. 3d) shows the presence of crystalline facets with atomic steps and kinks at the highly curved surface, highlighted by red and green lines, which are distinct from NPs with well-defined facets.[29–31] The result implies that OM-YS Au@AgPd NPs may have high catalytic performance on the electro-oxidation of ethanol.

The open-mouthed morphology of as-prepared OM-YS NPs was further confirmed by the energy dispersive spectroscopy (EDS) mapping of high-angle annular dark field-scanning transmission electron microscope (HDAAF-STEM) images (Fig. 4). The elemental distributions in HAADF-STEM-EDS mapping images (Fig. 4a–d) demonstrate that yolk–shell NPs are composed of elements Au, Ag and Pd. The element Au forms the yolk and its distribution shows a smaller circular shape (Fig. 4b); the element Pd and Ag form the shell and their distributions both show a bigger circular shape with missing gap (Fig. 4c and d). The overlapped image shows the open-mouthed structure (Fig. 4a). The HAADF-STEM-EDS mapping images of the conventional YS Au@AgPd NPs (Fig. S8a–d, ESI†) show that each element (Au, Pd and Ag) exhibits spherical shape; there is no open-mouth in the overlapped image.

In addition, the difference in the element composition and structure of the OM-YS Au@AgPd NP and the conventional YS Au@AgPd NPs was further confirmed by cross-sectional compositional line profiles (Fig. 4e and S8e, ESI†).

On the basis of the results obtained (Fig. 4 and S8, ESI†), as-prepared OM-YS and conventional YS Au@AgPd NPs can be given as OM-YS $Au_{0.70}@Ag_{0.17}Pd_{0.13}$ NPs and conventional YS $Au_{0.42}@Ag_{0.33}Pd_{0.25}$ NPs, respectively. Moreover, the Ag-to-Pd molar ratios in the AgPd shells of both NPs are nearly the same (about 1.3) though the contents of the Ag and Pd elements are different due to the difference in AgPd thickness. The EDS mapping results indicate that while OM-YS Au@AgPd NPs contain a lower amount of Ag (Fig. 4e), the amount of residual Ag in YS Au@AgPd NPs is fairly high (Fig. S8e, ESI†). The difference in residual silver amount between OM-YS and YS Au@AgPd NPs is further clearly reflected in the UV-vis absorption spectra of these NPs.

As in Fig. 5A, the surface plasmon resonance (SPR) peak of silver is still clearly visible in YS Au@AgPd NPs, which is blue-shifted from about 400 nm to about 380 nm after transformation of CS Au@Ag NPs to YS Au@AgPd ones. In the case of OM-YS Au@AgPd NPs, the Ag SPR peak, centered at about 400 nm, disappears while the new broad peak appears and is centered at about 345 nm. After the formation of AgPd shell *via* galvanic exchange reaction, the SPR peak of the Au yolks in the case of OM-YS Au@AgPd NPs red shifts from 509 to 519 nm, while it remain little changed in the case of YS Au@AgPd NPs.

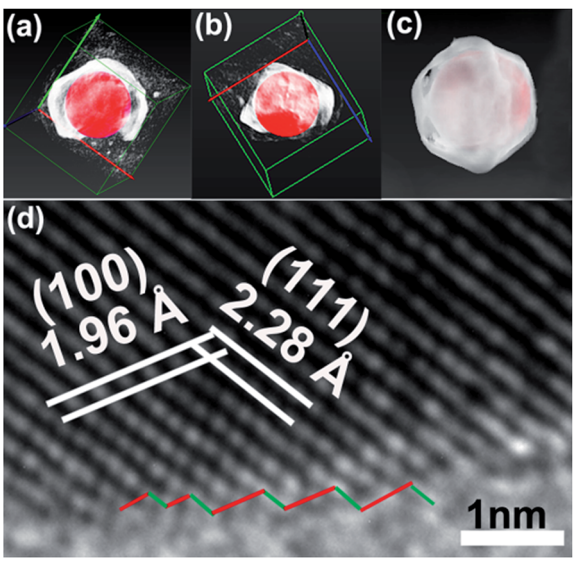

Fig. 3 3D reconstruction images (a and b) viewed from distinct angles, surface-rendered view reconstructed by the HAADF-STEM tomography (c) of an OM-YS Au@AgPd NP, HRTEM image (d) of the edge of a curved region of an OM-YS Au@AgPd NP (the inset in Fig. 2a).

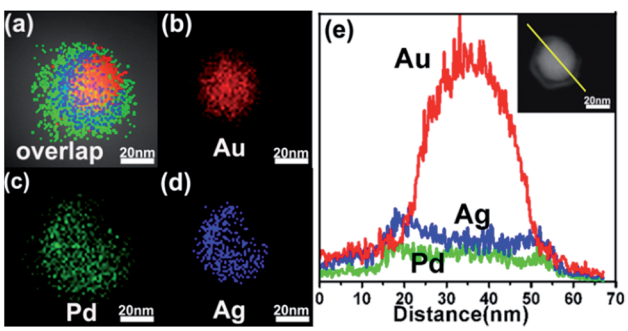

Fig. 4 High-angle annular dark field-scanning transmission electron microscope (HAADF–STEM) image (a), high-angle annular dark field-scanning transmission electron microscope-energy dispersive spectrometer (HAADF-STEM-EDS) mapping images (b, c and d) and cross-sectional compositional line profiles (e) of the OM-YS Au@AgPd NPs.

This journal is © The Royal Society of Chemistry 2015

Open Access Article. Published on 18 Mai 2015. Downloaded on 02.02.2026 10:12:41.
This article is licensed under a Creative Commons Attribution-NonCommercial 3.0 Unported Licence.

This suggest that the presence of the gap on the AgPd shells of OM-YS Au@AgPd NPs allow the exposure of Au yolks to the aqueous media, whereas the Au yolks of YS Au@AgPd NPs is well isolated by intact AgPd shells from the surrounding aqueous media. This spectroscopic difference is also reflected in the color difference between the aqueous dispersions of OM-YS Au@AgPd and YS Au@AgPd NPs dispersions; the dispersions of CS Au@Ag, YS Au@AgPd and OM-YS Au@AgPd NPs are orange, brown and purple, respectively (insets in Fig. 5A).

Fig. 5B shows the plots of the SPR peak positions of the Au yolks of YS Au@AgPd NPs and OM-YS Au@AgPd NPs *vs.* the refractive indexes of different solvents, respectively, in which the NPs are dispersed (details shown in Fig. S9a and b, ESI†).

It is well known that the SPR peak of Au NPs is sensitive to the refractive index of their dispersion medium.[32] It is obvious that the SPR peak positions of the Au yolks of OM-YS Au@AgPd NPs linearly increase with the refractive indexes of the dispersion solvents. This strongly underlines that the Au yolks are in direct contact with the dispersion media due to big gaps on the AgPd shells. In the case of YS Au@AgPd NPs, the change of the dispersion solvent from polar solvents (water and ethanol) to less polar organic solvents (tetrahydrofuran (THF), chloroform and toluene) leads to a noticeable red-shift of the SPR peaks of the Au yolks, from *ca.* 512 nm to *ca.* 524 nm. However, the solvent change from water to ethanol (or from THF to chloroform and toluene) does not cause linear change in the SPR peaks of the Au yolks, suggesting that SPR peak shifts are possibly induced by the NP agglomeration due to solvents used and the Au yolks are well protected by the intact AgPd shells from the contact with the surrounding media. These results not only endorse the open-mouthed morphology of the AgPd shells of as-prepared OM-YS Au@AgPd NPs but also underline the possibility for the Au yolks to take part in the technical applications of the AgPd shells.

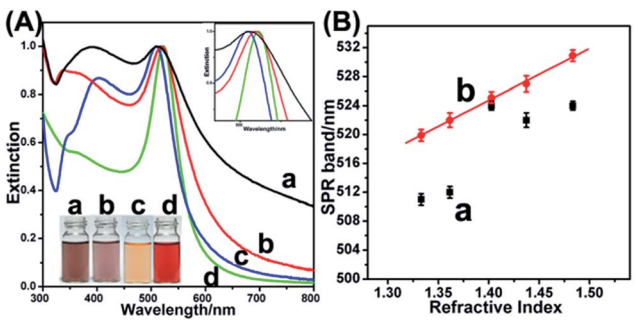

Fig. 5 The UV-vis spectra (A) of YS Au@AgPd NPs (a, black curve), OM-YS Au@AgPd NPs (b, red curve), CS Au@Ag NPs (c, blue curve) and Au NPs (d, green curve). The curves are normalized with the intensity of the SPR maximum of the Au NPs. The Au NPs are 30 nm in size. The insets in the lower-left corner are the optical photos of the glass vials of the aqueous dispersions of the corresponding NPs (a–d). The inset in the upper-right corner highlights the variation of the SPR maximum of the Au cores in different NPs. The plots of the peak positions (B) of Au cores in the conventional YS Au@AgPd NPs (a, solid square) and OM-YS Au@AgPd NPs (b, solid circle) *vs.* the refractive index of different solvents.

In our work, water-soluble sodium citrate was utilized to form the complexes with AgCl and, at the same time, stabilize as-prepared OM-YS or YS Au@AgPd NPs; no additional organic molecules were used as either chelating or stabilizing agents. Thus, the surfaces of the AgPd shells and Au yolks of as-prepared OM-YS Au@AgPd NPs are expected to be ligand-free after washing with water, this should be beneficial for catalysis.[21–23] Here we tested the catalytic performance of YS Au@AgPd NPs and OM-YS Au@AgPd NPs for electro-oxidation of ethanol in an alkaline medium. According to the literature,[33–35] OM-YS Au@AgPd NPs, YS Au@AgPd NPs, and commercially available Pd/C catalysts were utilized to modify glassy carbon electrodes (GCEs). The cyclic voltammetry (CV) measurement was carried out in 0.30 M N_2-saturated KOH aqueous solution at room temperature with a scan rate of 50 mV s^{-1} (Fig. S10, ESI†). The electrochemical active surface area (ECSA) of OM-YS Au@AgPd NP modified GCE electrodes are 87.8 $m^2\ g_{Pd}{}^{-1}$, which are about 1.8 and 2.9 times larger than the ECSAs of the GCEs modified by YS Au@AgPd NPs (49.6 $m^2\ g_{Pd}{}^{-1}$) and commercial Pd/C (30.4 $m^2\ g_{Pd}{}^{-1}$), respectively. The results underline that OM-YS Au@AgPd NPs are electrochemically more accessible, which is rather important for the electrocatalytic reactions. Comparing OM-YS Au@AgPd NPs with YS Au@AgPd NPs, the 1.8-fold increase in ECSA suggests that both the exterior and interior surfaces of the AgPd shells of the OM-YS Au@AgPd NPs take part in electrochemical reaction (Fig. S10, ESI†).

As compared with the nanoscale pores[19] (1–2 nm) on the AgPd shells of YS Au@AgPd NPs obtained, the average size of openings in the AgPd shells of as-prepared OM-YS Au@AgPd NPs is about 20 nm (as shown in Fig. 2), which is much larger than the mean free path of organic reactant molecules, thus leading to little diffusion resistance.[15] To exploit their potential use as anodes of direct ethanol fuel cells, OM-YS Au@AgPd NP-modified GCEs were used for electrocatalytic oxidation of ethanol. Fig. 6A shows the CV curves of GCEs modified by OM-YS Au@AgPd NPs, conventional YS Au@AgPd NPs and commercial Pd/C catalyst, respectively. OM-YS Au@AgPd NP-modified GCEs exhibit the less positive oxidation peak, centered at −0.214 V, suggesting a higher electrocatalytic activity. The mass normalized current density is about 1.25 A $mg_{Pd}{}^{-1}$, which is about 1.2 times and about 6.3 times larger than that of the GCEs modified by conventional YS Au@AgPd NPs (1.03 A $mg_{Pd}{}^{-1}$) and commercial Pd/C catalyst (0.20 A $mg_{Pd}{}^{-1}$) in the positive-going scan, respectively. It is known that in AgPd alloys Ag can shift up the d-band center of Pd on the basis of d-band center theory.[36,37]

As such, the presence of Ag in the Pd shells of as-prepared NPs is expected to facilitate the adsorption of OH^- ions onto the NP surfaces and thus enhance their performance in electrocatalysis of ethanol oxidation. The high Ag content, on the other hand, is expected to cause competition between OH^- ions and ethanol in adsorption on the NP surfaces, thus slowing down the electrocatalysis of ethanol oxidation.[38–41] As such, since the Ag content of YS Au@AgPd NPs is significantly larger than that of OM-YS Au@AgPd NPs, the GCEs modified by the OM-YS Au@AgPd NPs show lower electrochemical potential for ethanol

Open Access Article. Published on 18 Mai 2015. Downloaded on 02.02.2026 10:12:41.
This article is licensed under a Creative Commons Attribution-NonCommercial 3.0 Unported Licence.

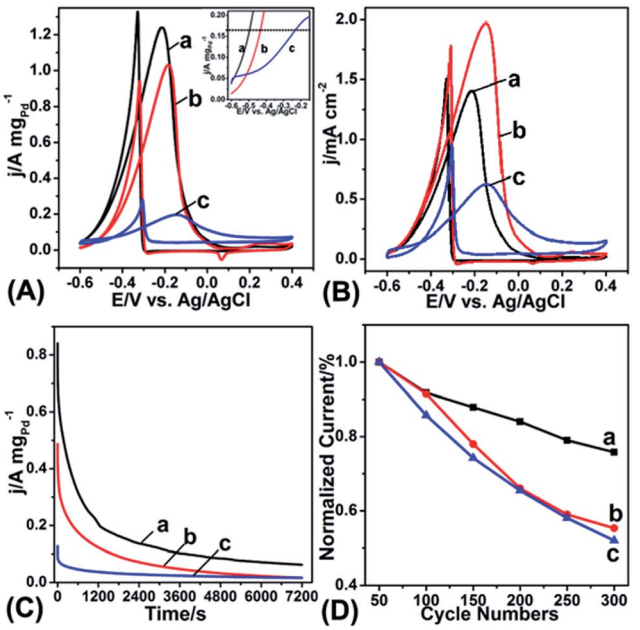

Fig. 6 CV curves (A), chronoamperometric curves (B) and potential cycling stability (C) of the GCEs modified by OM-YS Au@AgPd NPs (a, black curve), YS Au@AgPd NPs (b, red curve) and commercial Pd/C catalyst (c, blue curve) in 0.30 M N_2-saturated KOH aqueous solution at room temperature in the presence of 0.50 M ethanol. The currents shown in (A) and (B) both are normalized by the Pd mass loaded. The chronoamperometric curves (B) are recorded at −0.3 V. The scan rates of (A) and (C) are 20 and 50 mV s^{-1}, respectively.

oxidation than those modified by the conventional YS Au@AgPd NPs at the same oxidation current density (inset in Fig. 6A).

In order to assess the specific activity of OM-YS Au@AgPd NPs, YS Au@AgPd NPs and commercial Pd/C catalysts, the currents of their modified GCEs were also normalized by the ECSA values (Fig. 6B). The current density of OM-YS Au@AgPd NPs (1.4 mA cm^{-2}) is significantly higher than that of commercial Pd/C catalysts (0.65 mA cm^{-2}) while it is lower than that of YS Au@AgPd NPs (2.10 mA cm^{-2}). These results reveal that the average specific activity of either the inner surfaces of AgPd shells of OM-YS Au@AgPd NPs or their outer surfaces is lower than that of YS Au@AgPd NPs. Thus, the average mass-normalized current density of OM-YS Au@AgPd NPs is just slightly higher than that of YS Au@AgPd NPs. However, the presence of excess Ag is known to make Pd catalysts less stable due to the dissolution of excess Ag,[39–41] so the YS Au@AgPd NPs usually show poor durability (see below) even for our OM-YS Au@AgPd NPs with higher Ag amount, though their mass normalized current density can reach about 1.6 A mg_{Pd}^{-1} (Fig. S11†). Taking into account the durability of catalysts, therefore, we find the OM-YS Au@AgPd NPs with lesser Ag amount (1.25 A mg_{Pd}^{-1}) as the best samples.

To further assess and compare the catalysis durability of OM-YS Au@AgPd NPs, conventional YS Au@AgPd NPs and commercial Pd/C catalysts, the long-term electrocatalytic oxidation of ethanol was performed. On the basis of the chronoamperometric (CA) analysis shown in Fig. 6C, the electrochemical stability of OM-YS Au@AgPd NPs is superior to that of YS Au@AgPd NPs and commercial Pd/C catalysts; the commercial Pd/C catalysts undergo the most serious deactivation, most likely due to CO poisoning. At the end of 7200 s test, the oxidation current of GCEs modified by OM-YS Au@AgPd NPs is still 3.2 times larger than those modified by conventional YS Au@AgPd NPs. The potential cycling stability of GCEs modified by OM-YS Au@AgPd NPs, conventional YS Au@AgPd NPs and commercial Pd/C catalysts are also compared by using CV cycling, as shown in Fig. 6D. It can be seen that the oxidation peak current density of GCEs modified by OM-YS Au@AgPd NPs is only reduced to about 76% while that of conventional YS Au@AgPd NPs and commercial Pd/C catalysts is reduced to about 55 and 52%, respectively, after 300 cycles of electrochemical oxidation of ethanol. After the 300 cycling test, the thickness of the AgPd shells of conventional YS Au@AgPd NPs become thinner and some AgPd shells were totally dissolved (Fig. S12, ESI†) due to progressive dissolution of the higher amount of Ag in their shells into the solution, as Ag has a lower standard electrode potential than Pd.[39–41] In contrast, albeit dissolution of the AgPd shells is clearly visible in some NPs (Fig. S13a, ESI†), the majority of OM-YS Au@AgPd NPs still retain an OM-YS structural feature (Fig. S13b, ESI†) due to lesser amount of Ag in their shells. Taking into account the little difference in cycling stability between conventional YS Au@AgPd NPs and commercial Pd/C catalysts, the noticeably improved cycling stability and durability of OM-YS Au@AgPd NPs should be due to the fact that the surfaces of their Au yolks are in direct contact with the reaction media, which further improve CO tolerance. All of the results mentioned above indicate that OM-YS Au@AgPd NPs have a superior electrocatalytic activity for ethanol oxidation in alkaline media than conventional YS Au@AgPd NPs.

The electrocatalytic performances of a series of Pd-based NPs (such as core–shell $Au_{0.83}$@$Pd_{0.17}$ NPs, hollow $Ag_{0.73}Pd_{0.27}$ NPs and open-mouthed, hollow $Ag_{0.77}Pd_{0.23}$ NPs) were also performed (Fig. S14–S17, ESI†) for further comparison with OM-YS Au@AgPd NPs. The ECSAs of GCEs modified by CS Au@Pd NPs, hollow AgPd NPs and hollow AgPd NPs with open mouths are 29.5, 49.0 and 51.6 m^2 g_{Pd}^{-1}, respectively (Tables 1 and S5†). Accordingly, the mass normalized current density of OM-YS Au@AgPd NPs (1.25 A mg_{Pd}^{-1}) is about 2.6, 2.2 and 2.1 times larger than that of the GCEs modified by CS Au@AgPd NPs (0.48 A mg_{Pd}^{-1}), hollow AgPd NPs (0.58 A mg_{Pd}^{-1}) and hollow AgPd NPs with open mouths (0.595 A mg_{Pd}^{-1}) in the positive-going scan, respectively. These results further demonstrate that OM-YS Au@AgPd NPs have a superior electrocatalytic activity for ethanol oxidation in alkaline media than NPs of other types due to the access to interior surfaces of the shells.

Table 1 summarizes the electrochemical performances of as-prepared Pd-based catalysts on ethanol oxidation. It is clearly observed that the ECSA of hollow AgPd NPs are nearly the same as that of conventional YS Au@AgPd NPs with comparable sizes, indicating that the interior surfaces of hollow NPs may not be involved the electrocatalytic reaction due to the absence of open mouths. However, the ECSA of hollow AgPd NPs with open mouths are still close to that of conventional YS Au@AgPd NPs with comparable sizes, suggesting that there are possibly no Pd

 This journal is © The Royal Society of Chemistry 2015

Open Access Article. Published on 18 Mai 2015. Downloaded on 02.02.2026 10:12:41.
This article is licensed under a Creative Commons Attribution-NonCommercial 3.0 Unported Licence.

Table 1 Summary of ECSAs, potential values of oxidation peak and current density normalized by Pd mass of GCE modified by open-mouthed, YS $Au_{0.70}@Ag_{0.17}Pd_{0.13}$ NPs, open-mouthed, hollow $Ag_{0.73}Pd_{0.27}$ NPs, conventional YS $Au_{0.42}@Ag_{0.33}Pd_{0.25}$ NPs, hollow $Ag_{0.78}Pd_{0.22}$ NPs, CS $Au_{0.83}@Pd_{0.17}$ NPs and commercial Pd/C catalyst on ethanol oxidation in 0.30 M KOH solution containing 0.50 M ethanol, respectively

Samples	*E*/V	ECSA/$m^2\ g^{-1}$	Mass activity/A mg_{Pd}^{-1}
Open-mouthed, YS $Au_{0.70}@Ag_{0.17}Pd_{0.13}$ NPs	−0.214	87.8	1.25
Open-mouthed, hollow $Ag_{0.73}Pd_{0.27}$ NPs	−0.18	49.0	0.595
Conventional YS $Au_{0.42}@Ag_{0.33}Pd_{0.25}$ NPs	−0.180	49.6	1.03
Hollow $Ag_{0.78}Pd_{0.22}$ NPs	−0.211	51.6	0.58
CS $Au_{0.83}@Pd_{0.17}$ NPs	−0.206	29.5	0.48
Pd/C catalyst	−0.144	30.4	0.20

atoms on the interior surfaces of AgPd shells because the open mouths of hollow AgPd NPs are obtained by dissolution of Ag with H_2O_2. Thus, the interior surfaces of hollow AgPd NPs with open mouths contributed little to their catalytic performance, though they bear open mouths. In contrast, the ECSA of our OM-YS Au@AgPd NPs is twice as much as that of conventional YS Au@AgPd NPs, meaning that there are Pd atoms on the interior surfaces of AgPd shells of our OM-YS Au@AgPd NPs. Thus, only YS NPs with both open mouths and interior surfaces containing Pd atoms can have increased ECSA and enhanced electrocatalytic performance. To date, to our best knowledge, only our method enables the synthesis of YS Au@AgPd NPs of open-mouthed type.

The durability of the catalysts is also important for their electrocatalytic performance. Since the presence of Ag can not only promote the mass activity but also affect their durability due to the dissolution of excess Ag, OM-YS Au@AgPd NPs with lesser Ag amount (1.25 A mg_{Pd}^{-1}) were selected rather than the ones with higher Ag amount (1.6 A mg_{Pd}^{-1}) for this study. Conventional YS Au@AgPd NPs with higher Ag amount (1.03 A mg_{Pd}^{-1}) were selected in this work to demonstrate the negative effect of Ag, though they can have better mass activity. Consequently, the selected OM-YS Au@AgPd NPs in this work have an enhanced durability besides improved mass activity, compared to conventional YS Au@AgPd NPs with best mass activity.

Due to the presence of the open mouths on the shells of OM-YS Au@AgPd NPs, the Au yolks are in direct contact with surrounding media, which should improve their anti-CO poisoning ability and contribute to their durability. To understand the structure and composition effect on the anti-CO poisoning ability,[38,42] a series of CO-stripping voltammetry experiments were further performed (Fig. 7 and S18†). Pd in the Pd/C catalysts or core–shell Au@Pd NPs shows a pronounced and sharp CO oxidation peak at ~−0.2 V (Fig. 7a and b). Only one large diffuse peak from −0.6 to 0.1 V in the CV of the OM-YS Au@AgPd NPs was observed (Fig. 7c). This may be attributed to the fact that some Pd on the surfaces has not been alloyed with Ag due to the smaller amount of Ag on the surfaces.[38] The CV of the conventional YS Au@AgPd NPs show one tiny diffuse peak associated with CO oxidation due to formation of Pd–Ag alloy on the surfaces (Fig. 7d). Although some CO can be absorbed on the shells of OM-YS Au@AgPd NPs, CO oxidation peaks are found to disappear after stripping.

It is well known that Au is a good catalyst for CO oxidation. On the basis of the results reported in the literautre,[43,44] CO can largely adsorb on the surfaces of Au NPs and can be removed by reaction with the active oxygen species adsorbed on the Au NPs to form CO_2. The additional oxygen species are H_2O and OH^- ion in general. Thus, in our case, the CO_{ads} would be oxidized *via* the following reactions in alkaline media,[27]

$$CO_{ads} + Au\text{–}OH_{ads} \rightarrow Au\text{–}CO\text{–}OH \rightarrow Au\text{–}COOH \rightarrow Au + CO_2 + H_2O$$

Accordingly, the degradation and dehydrogenation of ethanol mainly occur on the exterior and interior surfaces of AgPd shells and CO-like intermediate species would oxidize on the surfaces of Au yolks to produce CO_2,[45] thus improving anti-CO poisoning ability of our OM-YS Au@AgPd NPs. Thus, OM-YS Au@AgPd NPs show higher activity and good stability for the oxidation of ethanol. Furthermore, a higher ratio of Ag on the AgPd shells can prohibit the CO adsorption at the initial stage (Fig. 7d), however, the exposed Pd shells are easily poisoned after Ag dissolution at later stage.[39–41] Thus, the stability of conventional YS Au@AgPd NPs becomes worse (Fig. S12, ESI†).

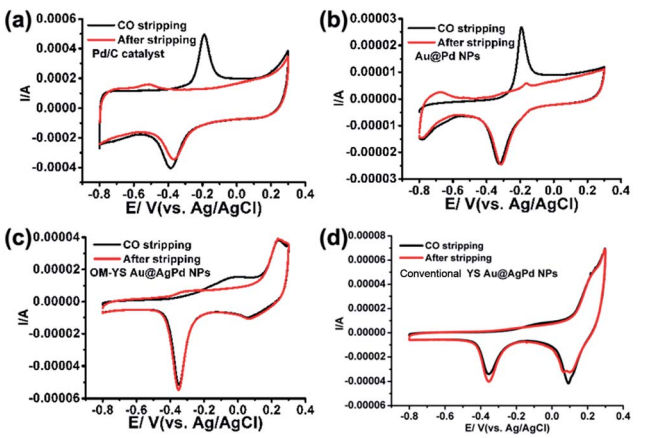

Fig. 7 CO stripping measurements of commercial Pd/C catalysts (a), CS Au@Pd NPs (b), open-mouthed, YS Au@AgPd NPs (c) and conventional YS Au@AgPd NPs (d), performed in a solution of 0.30 M KOH at 50 mV s^{-1}.

Open Access Article. Published on 18 Mai 2015. Downloaded on 02.02.2026 10:12:41.
This article is licensed under a Creative Commons Attribution-NonCommercial 3.0 Unported Licence.

Conclusions

In summary, we have successfully synthesized OM-YS Au@AgPd NPs *via* galvanic replacement reaction at room temperature after careful optimization of the Ag shell thickness of original CS Au@Ag NPs, citrate concentration, and the molar ratio of Pd^{2+} to Ag (about equal to 0.5). The surfaces of the AgPd shells of as-prepared OM-YS Au@AgPd NPs are noticeably rougher than those of conventional YS Au@AgPd NPs and containing a larger fraction of high index facets, which lead to superior catalytic activity for electrochemical oxidation of ethanol in alkaline media. Thanks to large single openings on the AgPd shells, both the exterior and interior surfaces of AgPd shells can be utilized for catalysis, thus leading to very large ECSA (up to 87.8 $m^2 g^{-1}$). In addition, the openings on the AgPd shells enable the Au yolks to be directly exposed to reaction media and facilitate the removal of CO and other carbonaceous intermediate species, and thus significantly enhance durability and stability of the AgPd shells. Overall, this open-mouthed yolk–shell nanoparticulate structure provides a genuine opportunity to integrate the functions of both shells and cores into unprecedented synergetic collective properties, which may result in significant advances not only in catalysis, as demonstrated here, but also in photonics, especially plasmonic optics, electrooptics, magnetics and many others.

Acknowledgements

This work is financially supported by the Natural Science Foundation of China (51172126, 21473105, 51002086, 51227002 and 51272129) and Shandong Provincial Natural Science Foundation for Distinguished Young Scientists (JQ201405). H. X. is grateful to the Program for New Century Excellent Talents in University (NCET-10-0553). D. W. thanks the Australian Research Council for financial support (DP 120102959120102959).

Notes and references

1 C. W. Xu, H. Wang, P. K. Shen and S. P. Jiang, *Adv. Mater.*, 2007, **19**, 4256–4259.
2 C. Bianchini and P. K. Shen, *Chem. Rev.*, 2009, **109**, 4183–4206.
3 G. J. Zhang, Y. E. Wang, X. Wang, Y. Chen, Y. M. Zhou, Y. W. Tang, L. D. Lu, J. C. Bao and T. H. Lu, *Appl. Catal., B*, 2011, **102**, 614–619.
4 F. L. Cheng, X. C. Dai, H. Wang, S. P. Jiang, M. Zhang and C. W. Xu, *Electrochim. Acta*, 2010, **55**, 2295–2298.
5 L. Y. Chen, N. Chen, Y. Hou, Z. C. Wang, S. H. Lv, T. Fujita, J. H. Jiang, A. Hirata and M. W. Chen, *ACS Catal.*, 2013, **3**, 1220–1230.
6 Y. W. Lee, M. J. Kim, Y. Kim, S. W. Kang, J.-H. Lee and S. W. Han, *J. Phys. Chem. C*, 2010, **114**, 7689–7693.
7 L. F. Zhang and C. Y. Zhang, *Nanoscale*, 2013, **5**, 6074–6080.
8 G. H. Jeong, D. Choi, M. Kang, J. Shin, J. G. Kang and S. W. Kim, *RSC Adv.*, 2013, **3**, 8864–8870.
9 S. Shen, T. S. Zhao, J. Xu and Y. Li, *Energy Environ. Sci.*, 2011, **4**, 1428–1433.
10 D. Kim, Y. W. Lee, S. B. Lee and S. W. Han, *Angew. Chem., Int. Ed.*, 2012, **51**, 159–163.
11 J. Liu, S. Z. Qiao, J. S. Chen, X. W. Lou, X. R. Xing and G. Q. Lu, *Chem. Commun.*, 2011, **47**, 12578–12591.
12 C. Guan, X. Xia, N. Meng, Z. Zeng, X. Cao, C. Soci, H. Zhang and H. J. Fan, *Energy Environ. Sci.*, 2012, **5**, 9085–9090.
13 X. Y. Lai, J. E. Halpert and D. Wang, *Energy Environ. Sci.*, 2012, **5**, 5604–5618.
14 C. Chen, Y. J. Kang, Z. Y. Huo, Z. W. Zhu, W. Y. Huang, H. L. Xin, J. D. Snyder, D. G. Li, J. A. Herron, M. Mavrikakis, M. F. Chi, K. L. More, Y. D. Li, N. M. Markovic, G. A. Somorjai, P. D. Yang and V. R. Stamenkovic, *Science*, 2014, **343**, 1339–1343.
15 Y. Yamauchi, A. Tonegawa, M. Komatsu, H. J. Wang, L. Wang, Y. Nemoto, N. Suzuki and K. Kuroda, *J. Am. Chem. Soc.*, 2012, **134**, 5100–5109.
16 M. A. Mahmoud, R. Narayanan and M. A. El-Sayed, *Acc. Chem. Res.*, 2013, **46**, 1795–1805.
17 X. Xia, Y. Wang, A. Ruditskiy and Y. Xia, *Adv. Mater.*, 2013, **25**, 6313–6333.
18 E. González, J. Arbiol and V. Puntes, *Science*, 2011, **334**, 1377–1380.
19 L. Kuai, B. Geng, S. Wang and Y. Sang, *Chem.–Eur. J.*, 2012, **18**, 9423–9429.
20 S. Wang, L. Kuai, Y. Huang, X. Yu, Y. Liu, W. Li, L. Chen and B. Geng, *Chem.–Eur. J.*, 2013, **19**, 240–248.
21 H. Zhang, M. Jin, Y. Xiong, B. Lim and Y. Xia, *Acc. Chem. Res.*, 2013, **46**, 1783–1794.
22 X. Hong, D. Wang, S. Cai, H. Rong and Y. Li, *J. Am. Chem. Soc.*, 2012, **134**, 18165–18168.
23 W. Zhang, J. Yang and X. Lu, *ACS Nano*, 2012, **6**, 7397–7405.
24 H. Li, H. Xia, D. Wang and X. Tao, *Langmuir*, 2013, **29**, 5074–5079.
25 W. Wang, J. Zhang, S. Yang, B. Ding and X. Song, *ChemSusChem*, 2013, **6**, 1945–1951.
26 H. Wang, Z. Sun, Y. Yang and D. Su, *Nanoscale*, 2013, **5**, 139–142.
27 L. Chen, N. Chen, Y. Hou, Z. Wang, S. Lv, T. Fujita, J. Jiang, A. Hirata and M. Chen, *ACS Catal.*, 2013, **3**, 1220–1230.
28 D. A. Slanac, W. G. Hardin, K. P. Johnston and K. J. Stevenson, *J. Am. Chem. Soc.*, 2012, **134**, 9812–9819.
29 H. Xia, Y. Ran, H. Li, X. Tao and D. Wang, *J. Mater. Chem. A*, 2013, **1**, 4678–4684.
30 N. Tian, Z. Zhou, S. Sun, Y. Ding and Z. Wang, *Science*, 2007, **316**, 732–735.
31 T. Fujita, P. Guan, K. McKenna, X. Lang, A. Hirata, L. Zhang, T. Tokunaga, S. Arai, Y. Yamamoto, N. Tanaka, Y. Ishikawa, N. Asao, Y. Yamamoto, J. Erlebacher and M. Chen, *Nat. Mater.*, 2012, **11**, 775–780.
32 J. Pérez-Juste, I. Pastoriza-Santos, L. Liz-Marzán and P. Mulvaney, *Coord. Chem. Rev.*, 2005, **249**, 1870–1901.
33 S. Guo, S. Dong and E. Wang, *Energy Environ. Sci.*, 2010, **3**, 1307–1310.
34 L. Xiao, L. Zhuang, Y. Liu, J. Lu and H. Abruna, *J. Am. Chem. Soc.*, 2009, **131**, 602–608.
35 Y. Xu, R. Xu, J. Cui, Y. Liu and B. Zhang, *Chem. Commun.*, 2012, **48**, 3881–3883.

 This journal is © The Royal Society of Chemistry 2015

Open Access Article. Published on 18 Mai 2015. Downloaded on 02.02.2026 10:12:41.
This article is licensed under a Creative Commons Attribution-NonCommercial 3.0 Unported Licence.

36 B. Hammer and J. Nørskov, *Adv. Catal.*, 2000, **45**, 71–129.
37 J. Greeley, J. Nørskov and M. Mavrikakis, *Annu. Rev. Phys. Chem.*, 2002, **53**, 319–348.
38 S. Nguyen, H. Law, H. Nguyen, N. Kristian, S. Wang, S. Chan and X. Wang, *Appl. Catal., B*, 2009, **91**, 507–515.
39 Z. Peng, H. You and H. Yang, *Adv. Funct. Mater.*, 2010, **20**, 3734–3741.
40 H. Ji, J. Frenzel, Z. Qi, X. Wang, C. Zhao, Z. Zhang and G. Eggeler, *CrystEngComm*, 2010, **12**, 4059–4062.
41 D. R. Lide, *CRC Handbook of Chemistry and Physics*, CRC Press/Taylor and Francis, Boca Raton, FL, USA, 88th edn, 2007.
42 A. Wang, H. Xu, J. Feng, L. Ding, Y. Tong and G. Li, *J. Am. Chem. Soc.*, 2013, **135**, 10703–10709.
43 A. Wittstock and M. Bäumer, *Acc. Chem. Res.*, 2014, **47**, 731–739.
44 D. Widmann and J. Behm, *Acc. Chem. Res.*, 2014, **47**, 740–749.
45 J. Datta, A. Dutta and S. Mukherjee, *J. Phys. Chem. C*, 2011, **115**, 15324–15334.